Journal of Applied Physics ARTICLE scitation.org/journal/jap

Understanding the effects of iodine doping on the thermoelectric performance of n-type PbTe ingot materials

Cite as: J. Appl. Phys. **126**, 025108 (2019); doi: 10.1063/1.5101034
Submitted: 23 April 2019 · Accepted: 22 June 2019 ·
Published Online: 11 July 2019

View Online Export Citation CrossMark

Juan Cui,[1,2] Meimei Wang,[1] Xiao Xu,[1] Yue Chen,[2] and Jiaqing He[1,a)]

AFFILIATIONS

[1]Shenzhen Key Laboratory of Thermoelectric Materials, Department of Physics, Southern University of Science and Technology, Shenzhen 518055, China
[2]Department of Mechanical Engineering, The University of Hong Kong, Pokfulam Road, Hong Kong SAR, China

Note: This paper is part of the special topic on Advanced Thermoelectrics.
[a)]**Email:** hejq@sustech.edu.cn

ABSTRACT

The superior performance of p-type PbTe has generated excitement toward discovering an n-type PbTe recipe to meet the manufacturing requirements for thermoelectric devices. PbI_2 is a well-known dopant for n-type PbTe alloys fabrication. For the halogen family, the sintering process involves a common densifying strategy used to reduce the lattice thermal conductivity, which unfortunately causes strong deviations from nominal composition. Thus, to precisely determine the effects of iodine on PbTe's electrical properties, PbI_2-doped ingots were fabricated and characterized in this work. We found that the ingot samples exhibited high electrical conductivity, high power factors, and low lattice thermal conductivity when x equaled 0.004 and 0.005, especially at low temperatures, which was comparable with previous reports.

I. INTRODUCTION

The global energy crisis is a major social and economic issue, and people have directed significant effort to finding sustainable alternative energy sources, including solar, nuclear, and bioenergy. Thermoelectric materials have intrigued researchers as they can readily allow reversible conversion between heat and electricity.[1] The energy conversion process is only triggered by a temperature gradient and the energy conversion efficiency depends on a dimensionless figure of merit (ZT): $ZT = \frac{S^2\sigma}{\kappa_l+\kappa_e}T$, where S, σ, T, κ_l, and κ_e are the Seebeck coefficient, electrical conductivity, temperature in kelvin, lattice thermal conductivity, and electronic thermal conductivity, respectively. An ideal thermoelectric material should simultaneously have a high power factor ($S^2\sigma$) and a low thermal conductivity ($\kappa_l + \kappa_e$), but these parameters are interrelated, making property optimization complicated and difficult.[2] Doping,[3] alloying,[4] and nanostructuring[5] are widely used methods to tune these two parameters. Most effort has been devoted to improving the peak ZT, while for thermoelectric devices, a high average ZT (ZT_{ave}) plays an important role since it is directly related to the heat-electricity conversion efficiency of a device (η) as the following equations show:

$$\eta = \frac{T_h - T_c}{T_h}\left[\frac{\sqrt{1+ZT_{ave}}-1}{\sqrt{1+ZT_{ave}}+T_c/T_h}\right], \quad (1)$$

$$ZT_{ave} = \frac{1}{T_h - T_c}\int_{T_c}^{T_h} ZT dT, \quad (2)$$

where T_h and T_c are the temperatures at the hot and cold extremes, respectively. If T_h and T_c are fixed, η increases with ZT_{ave}.[6] To obtain a high ZT_{ave}, enhancing the ZT at low temperature is important.

To date, various classes of thermoelectric materials have been developed, such as Bi_2Te_3 for low temperature applications[7,8] and GeTe for higher temperature applications.[9] PbTe-based compounds are typical moderate-temperature thermoelectric materials that

work between 300 K and 800 K, which are proposed to have high ZT_{ave} values.[10] Recent studies on p-type PbTe, such as Na-doped $PbTe_{0.8}S_{0.2}$[11] and $PbTe_{0.85}Se_{0.15}$–2Na–4SrTe,[5] have shown a peak ZT of 2.3 at 923 K, which is higher than that of n-type PbTe materials. The highest ZT of n-type PbTe was 1.8 at 773 K, as reported by Fu *et al.*[12] Moreover, LaLonde *et al.* found a $ZT \sim 1.4$ between 700 K and 850 K in PbI_2-doped PbTe,[13] and Bali *et al.* achieved a $ZT \sim 1.12$ in In-doped PbTe at 773 K.[14] Therefore, there is still much room for improvement in n-type PbTe materials in terms of ZT. As a well-known n-type dopant in PbTe, PbI_2 has been widely investigated for decades.[15–17] However, due to the drastic sintering process, the final composition of materials doped with this is difficult to control and often deviates from the nominal composition. Therefore, in this study, we optimized the carrier concentration of ingot $PbTe_{1-x}I_x$ ($x = 0$, 0.002, 0.003, 0.004, 0.005) samples to study the effects of iodine on PbTe.

Furthermore, by comparing an ingot sample of $PbTe_{0.996}I_{0.004}$ with other halide-doped PbTe samples from the literature,[13,14,18,19] we found that the ingot sample in this study was among the best n-type halide-doped PbTe material in terms of both ZT and ZT_{ave}. Hall measurements and optical microscopy were used to analyze its performance. To date in the literature, most ZT_{ave} values reported for halide-doped PbTe materials in the temperature range 373–660 K are less than 0.9, such as 0.68 for In- and I-doped PbTe,[14] 0.85 for $PbTe_{1-x}I_x$ reported by LaLonde *et al.*,[13] and 0.59 for Cl doped $(PbTe)_{0.75}(PbS)_{0.15}(PbSe)_{0.1}$.[18] Hence, this study is of great significance for the practical application of PbTe-based materials.

II. EXPERIMENTAL DETAILS

A. Sample preparation

In this study, samples with stoichiometric compositions of $PbTe_{1-x}I_x$ ($x = 0$, 0.002, 0.003, 0.004, 0.005) were synthesized by mixing corresponding ratios of high-purity Pb (99.99%), Te (99.99%), and PbI_2 in carbon-coated quartz tubes. Raw materials were flame-sealed in carbon-coated quartz tubes under a pressure of $\sim 10^{-4}$ Pa at room temperature. These tubes were then heated to 1273 K slowly in 12 h, held at this temperature for 6 h, and cooled to room temperature naturally in a program-controlled furnace. Quenching or annealing was not involved. After cooling, the cylinder ingots were taken out and cut into specific shapes for further property measurements.

B. Sample characterization

Phase information was obtained using X-ray powder diffraction (XRD) (Rigaku, MiniFlex 600) with Cu K_α radiation at a scanning rate of $4° \text{ min}^{-1}$. The cylinder ingots were cut into cuboids with the dimensions $3 \times 3 \times 10$ mm^3. The Seebeck coefficient and the electrical conductivity were measured simultaneously using a Ulvac Riko ZEM-3 instrument from 323 K to 773 K under a helium atmosphere. The uncertainty was about 5% for the electrical conductivity and Seebeck coefficient measurements. Disks with a diameter of 10 mm and a thickness of 1–2 mm were cut from the cylinder ingots for the measurement of thermal diffusivity (D) in the 323–773 K temperature range with a Netzsch LFA467 apparatus. Thermal conductivities were calculated according to the formula $\kappa = D \times d \times C_p$, where d is the density obtained by the Archimedes method and C_p is the specific heat capacity estimated by the Dulong-Petit law. The total uncertainty of the thermal conductivity was about 10%.

Hall coefficients (R_H) were measured by the van der Pauw method in a magnetic field of 0.8 T in a commercial Hall measurement system (Lake Shore 8400 Series) at room temperature. The effective carrier concentration (n_H) was calculated by $n_H = 1/(eR_H)$, with e being the elemental charge, and the Hall mobility (μ_H) was calculated by $\mu_H = \sigma R_H$, where σ represents the electrical conductivity obtained from the ZEM-3 instrument.

A hot corrosion experiment was performed on a polished $PbTe_{0.996}I_{0.004}$ sample with a program-controlled furnace. The furnace was heated from room temperature to 673 K in 40 min, held at this temperature for 20 min and then cooled naturally to room temperature. The pressure of the chamber was lower than 10^{-2} Pa during the whole process. After hot corrosion, the sample surface showed different coloration and was further observed under an optical microscope.

III. RESULTS AND DISCUSSION

A. Phase analysis

Figure 1 shows the XRD patterns of $PbTe_{1-x}I_x$ ($x = 0$, 0.002, 0.003, 0.004, and 0.005) samples. The presence of one set of peaks indicates that only one phase was formed, and the phase was indexed to the rock-salt structure ($Fm\bar{3}m$) according to the standard card (PDF#38-1435). As x increased, the positions of the diffraction peaks were nearly unchanged, similar to the enlarged (200) peak shown in Fig. 1(b), which was understandable since the radius of I^- was close to that of Te^{2-} and the doping level of iodine was very low.

B. Thermoelectric properties

Figure 2 depicts the temperature-dependent thermoelectric properties of $PbTe_{1-x}I_x$ ingots. As shown in Fig. 2(b), the pristine PbTe sample was p-type, with a positive Seebeck coefficient in the

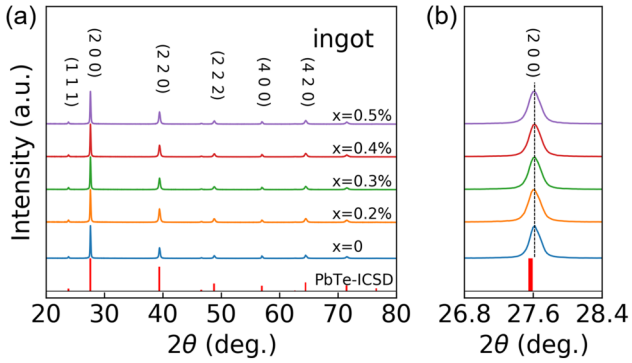

FIG. 1. (a) Powder XRD patterns for samples of $PbTe_{1-x}I_x$ ($x = 0$, 0.002, 0.003, 0.004, and 0.005). (b) An enlarged view of the (200) Bragg peak. A dashed vertical line was used as a reference.

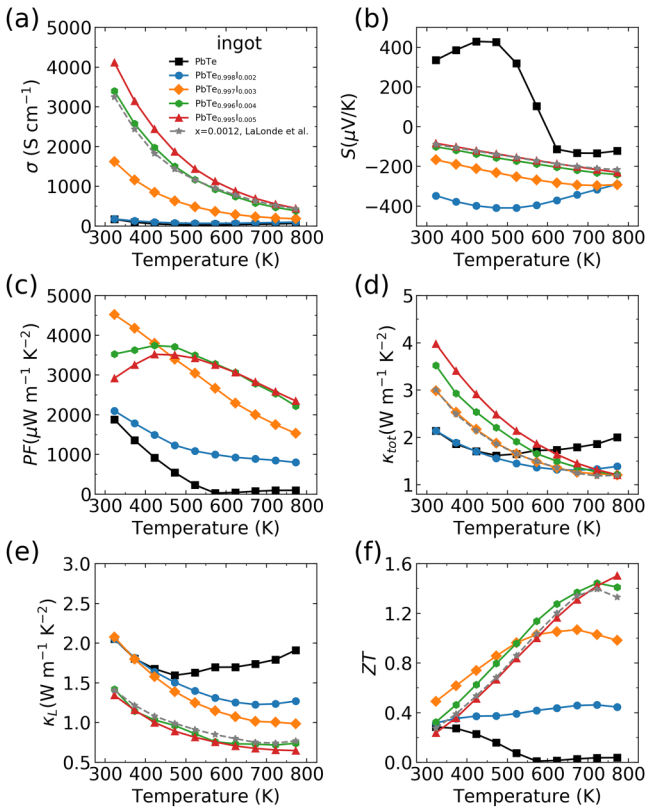

FIG. 2. Temperature-dependent transport properties of $PbTe_{1-x}I_x$ ($x = 0$, 0.002, 0.003, 0.004, and 0.005), compared to LaLonde's sample at $x = 0.0012$:[13] (a) electrical conductivity, (b) Seebeck coefficient, (c) power factor, (d) thermal conductivity, (e) lattice thermal conductivity, and (f) *ZT*.

low temperature range. With iodine doped in, the samples turn to n-type and the absolute *S* values decreased gradually with increasing iodine content. For the sample where $x = 0.002$, the absolute *S* value dropped distinctly when the temperature was higher than 500 K, mainly due to the early appearance of thermal excited minority carriers. On the other hand, all the samples showed a decrease in the electrical conductivity at elevated temperatures [Fig. 2(a)]. As the iodine content increased, the electrical conductivity increased dramatically at low temperatures, which indicated that iodine has been successfully doped into the matrix. This ultrahigh electrical conductivity and the competitive Seebeck coefficient benefit the power factor, as shown in Fig. 2(c). The largest power factor was achieved when $x = 0.003$ at 300 K ($4519\,\mu W\,m^{-1}\,K^{-2}$), while the sample with $x = 0.004$ had a larger average power factor over the whole temperature range, reaching a fine balance between *S* and σ. The electrical conductivities of the ingot samples at room temperature in this work were much higher than the reported values in In and I codoped samples ($2500\,S\,cm^{-1}$)[14] or n-type $Pb_{1-x}Bi_xTe$ ($2300\,S\,cm^{-1}$) and $Pb_{1-x}Sb_xTe$ ($\sim 2000\,S\,cm^{-1}$),[20] contributing significantly to a larger ZT_{ave}.

The total thermal conductivities of all the doped samples obviously decreased as the temperature increased from 323 K to 600 K and were gradually saturated from 600 K to 773 K, which was consistent with the trend for the electrical conductivity [Fig. 2(d)]. The thermal conductivity of the pristine sample increased at temperatures above 500 K due to the bipolar effect. As iodine content increased, the total thermal conductivity obviously increased and was dominated by the electronic thermal conductivity, which was proportional to the electrical conductivity ($\kappa_{ele} = L\sigma T$). On the other hand, the lattice thermal conductivity [Fig. 2(e)] gradually decreased as the iodine content increased and the lowest value was comparable with that of LaLonde's sample at $x = 0.0012$, which was fabricated with annealing, grounding, and hot-pressing.[13] Apart from the lattice thermal conductivity, the electrical transport properties and the *ZT* of the $x = 0.004$ sample in this work were also close to those of LaLonde's sample at $x = 0.0012$ over the entire temperature range. Gelbstein *et al.* indicated that an optimal power factor could be obtained in a sintered PbTe sample at a level close to that of cast and single-crystal samples.[21] It can be seen from Fig. 2(f) that the highest *ZT* was achieved at a composition of $x = 0.005$ at 773 K, while the highest ZT_{ave} was achieved when $x = 0.004$. Because ZT_{ave} was more significant to the practical application of n-type PbTe materials, the $x = 0.004$ sample will be further discussed.

C. Hall measurements

The carrier concentration, mobility, and density of ingot samples were measured and are shown in Table I. The pristine PbTe ingot had a much lower mobility than others since it was a p-type thermoelectric material with hole carriers. The effective mass of hole carriers is usually larger than that of the electrons. The mobilities for samples with $x = 0.002$–0.005 were all above $1000\,cm^2\,V^{-1}\,s^{-1}$, the highest among the n-type PbTe materials. As *x* increased from 0.002 to 0.005, the carrier concentration increased from $10^{18}\,cm^{-3}$ to $3.4 \times 10^{19}\,cm^{-3}$, indicating that iodine was a rather effective n-type dopant. Combining the XRD analysis shown in Fig. 1 and the thermoelectric performance shown in Fig. 2, we deduced that the optimal carrier concentration for a PbTe system can be realized by simply doping a small amount of iodine (~0.004) without affecting the lattice parameter. The optimal carrier concentration was about $2 \times 10^{19}\,cm^{-3}$, which was consistent with the optimal value obtained by Pei *et al.* in both I-doped PbTe and La-doped PbTe systems.[22] In the meantime, the densities of the samples doped with iodine were slightly larger than that of the pristine sample.

The carrier concentration dependent Hall mobilities are shown in Fig. 3. Compared with the literature, the mobility in this

TABLE I. Carrier concentration, mobility, and density of the $PbTe_{1-x}I_x$ ingots.

x	n ($10^{18}\,cm^{-3}$)	μ ($cm^2\,V^{-1}\,s^{-1}$)	Density ($g\,cm^{-3}$)
0	3.47	302	8.17
0.002	1.01	1150	8.23
0.003	9.29	1530	8.25
0.004	19.2	1200	8.25
0.005	34.3	1230	8.23

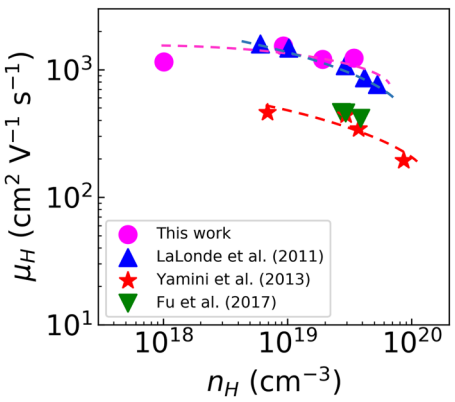

FIG. 3. Room temperature carrier concentration dependent Hall mobility of n-type PbTe in this work compared to those reported in the literature.[12,13,18]

work was close to that in LaLonde's work. This may account for their similar electrical transport properties as shown in Figs. 2(a) and 2(b). On the other hand, the mobility in this work was higher than that reported by Yamini *et al.* and Fu *et al.*, which may be related to the different formulations. The simple formula $PbTe_{1-x}I_x$ and the low doping concentration of iodine ensure a low defect scattering and low lattice strain, leading to a high electron mobility. On the other hand, alloying S results in a more localized carrier density distribution[17] and substituting Pb with Sb affects the band structure, which deteriorates the mobility.[12,23]

D. DFT calculations

To investigate the influence of iodine on the electronic structure of PbTe, the density of states (DOS) for I-doped PbTe was calculated. Computational details are included in the supplementary material. As shown in Fig. 4(a), the valence band of I-doped PbTe was dominated by the Te *5p* orbitals, while the conduction band

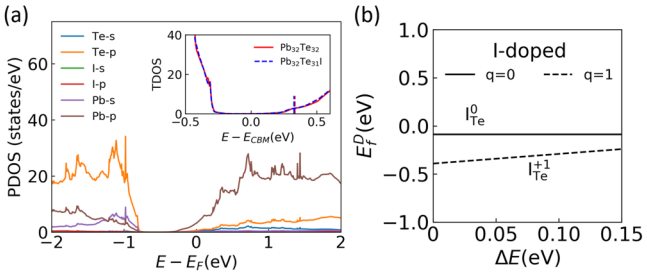

FIG. 4. (a) The projected density of states (PDOS) of I-doped PbTe. The inset shows the total density of states (TDOS) of PbTe and I-doped PbTe. The conduction band minima (CBM) were set to 0 eV for comparison. The vertical dashed lines represent the energy levels that correspond to a n-type carrier concentration of 10^{20} cm^{-3} for the different systems. (b) Defect formation energy of I_{Te} in PbTe. ΔE is the chemical potential relative to the valence band maximum (VBM).

was dominated by Pb *6p* orbitals. The contribution from the doped I atom was minor. By comparing the DOS of pristine PbTe and I-doped PbTe supercells, we observed the largely overlapped DOS near the CBM, which indicates that the doping iodine does not significantly affect the electronic structure of PbTe. On the other hand, the calculated bandgap was 0.146 eV, which was consistent with Tan's result.[24] The impurity formation energies for I_{Te} at different charge states [Fig. 4(b)] shows that I_{Te} was more stable in the +1 charge state, indicating that I_{Te} tended to be a donor in PbTe.

E. Microstructure

To further investigate the effects of iodine on a PbTe ingot, a hot corrosion method was employed on the $PbTe_{0.996}I_{0.004}$ sample. The optical microscopy images (Fig. 5) show that the grain size was larger than 1 mm and the size distribution was nonuniform. Pits and small holes existed on the surface, which was normal due to the hot corrosion process and the bubbles induced during the fabrication process. Compared with the nanoscale grain size of the hot-pressed samples reported by Bali *et al.*,[14] the grain size of the ingot was much larger. Normally, due to the larger grain size and fewer grain boundaries, the lattice thermal conductivity was higher because of less boundary scattering. However, as shown in Fig. 2(e), the lattice thermal conductivity of our ingot was comparable with that of LaLonde's sample, which was fabricated using hand grinding and hot-pressing. We show that the highest *ZT* value realized in our ingot samples was comparable to that of the hot-pressed samples of LaLonde. However, compared with other n-type PbTe systems, the lattice thermal conductivity of PbI_2-doped PbTe ingot was higher (see Fig. S1 in the supplementary material).[4,25,26]

F. Figure of merit (*ZT*)

As shown in Fig. 6, among the n-type PbTe samples doped with halides, the highest *ZT* of our ingots was comparable with that of LaLonde's work; however, the ZT_{ave} obtained was obviously larger than the others due to the excellent thermoelectric performance throughout the entire temperature range, which originated from the extremely high electrical conductivity. The ZT_{ave} of sample $x = 0.004$ was 0.89 in the 375–660 K temperature range, which was 75% larger than the value reported by Guch *et al.*[19] The properties of ingots in this work indicate that iodine was a very effective n-type dopant in PbTe and provide enough carrier concentration with a small doping amount without obviously affecting

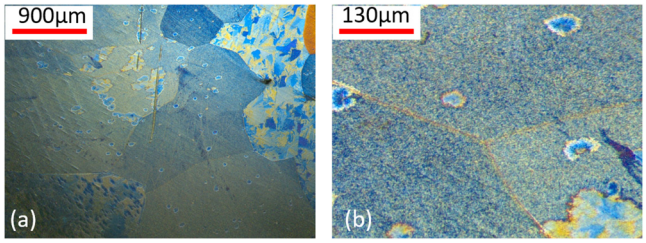

FIG. 5. (a) Optical microscopy images of a $PbTe_{0.996}I_{0.004}$ sample. (b) An enlarged image of the grain boundary shown in (a).

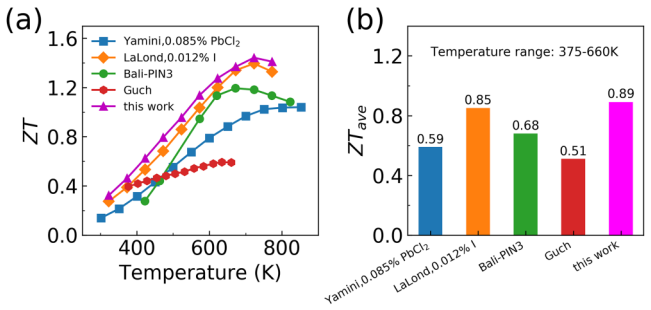

FIG. 6. Comparison of the (a) ZT values and (b) average ZT values of our samples with reported n-type PbTe samples doped with halides.[13,14,18,19]

the lattice structure. Thus, simply doping iodine with PbTe can be used to realize a high electrical conductivity with a high carrier mobility. Furthermore, by precisely controlling the iodine content, $PbTe_{1-x}I_x$ ingot samples with ZT and ZT_{ave} values competitive with the ground and hot-pressed samples could be realized.

IV. CONCLUSIONS

The advantages of doping iodine in PbTe were clearly demonstrated by studying the thermoelectric properties of $PbTe_{1-x}I_x$ ingots in this work. We found that iodine was an effective donor in PbTe that provides sufficient carrier concentration with a small dopant amount. Moreover, doping iodine did not affect the lattice structure significantly as the radius of I^- and Te^{2-} are close. These two factors ensured the high carrier concentration and the high mobility of $PbTe_{1-x}I_x$ simultaneously, contributing to a high electrical conductivity. We achieved a ZT of 1.4 at 773 K and a ZT_{ave} of 0.89 in the 375–660 K temperature range in a $PbTe_{0.096}I_{0.004}$ ingot, which was among the best n-type halide-doped PbTe thermoelectric materials. Our theoretical calculations also provided insight into the electronic structure to support our experimental observations. Compared with those reported in other studies, our ingot $PbTe_{1-x}I_x$ samples realized a competitive ZT and ZT_{ave} with ground and hot-pressed samples.

SUPPLEMENTARY MATERIAL

See the supplementary material for computational details and the comparison of lattice thermal conductivities with other n-type PbTe systems.

ACKNOWLEDGMENTS

This work was supported by the Natural Science Foundation of Guangdong Province (No. 2015A030308001), the leading talents of Guangdong Province Program (No. 00201517), the Science, Technology and Innovation Commission of Shenzhen Municipality (Nos. JCYJ20150831142508365, JCYJ20180307154619840, KQTD2016022619565991, and ZDSYS20141118160434515), and the National Natural Science Foundation of China (NNSFC) (Nos. 51632005, 11874194, and 51802146). We also acknowledge support from the Center for Computational Science and Engineering of Southern University of Science and Technology.

REFERENCES

[1]J. He and T. M. Tritt, Science **357**, eaak9997 (2017).
[2]T. Zhu, Y. Liu, C. Fu, J. P. Heremans, J. G. Snyder, and X. Zhao, Adv. Mater. **29**, 1605884 (2017).
[3]C. Long, X. Hou, Y. Gelbstein, J. Zhang, B. Ren, and Z. Wang, in *2006 25th International Conference on Thermoelectrics* (IEEE, 2006), p. 382.
[4]Y. Xiao *et al.*, Energy Environ. Sci. **11**, 2486 (2018).
[5]Y. Pei *et al.*, Adv. Energy Mater. **7**, 1601450 (2017).
[6]X. Zhang and L.-D. Zhao, J. Materiomics **1**, 92 (2015).
[7]R. Vizel, T. Bargig, O. Beeri, and Y. Gelbstein, J. Electron. Mater. **45**, 1296 (2016).
[8]O. Beeri, O. Rotem, E. Hazan, E. A. Katz, A. Braun, and Y. Gelbstein, J. Appl. Phys. **118**, 115104 (2015).
[9]E. Hazan, N. Madar, M. Parag, V. Casian, O. Ben-Yehuda, and Y. Gelbstein, Adv. Electron. Mater. **1**, 1500228 (2015).
[10]H. J. Wu, L. D. Zhao, F. S. Zheng, D. Wu, Y. L. Pei, X. Tong, M. G. Kanatzidis, and J. Q. He, Nat. Commun. **5**, 4515 (2014).
[11]D. Wu *et al.*, Energy Environ. Sci. **8**, 2056 (2015).
[12]L. Fu, M. Yin, D. Wu, W. Li, D. Feng, L. Huang, and J. He, Energy Environ. Sci. **10**, 2030 (2017).
[13]A. D. LaLonde, Y. Pei, and G. J. Snyder, Energy Environ. Sci. **4**, 2090 (2011).
[14]A. Bali *et al.*, J. Appl. Phys. **120**, 175101 (2016).
[15]M. Orihashi, Y. Noda, H. T. Kaibe, and I. A. Nishida, Mater. Trans. JIM **39**, 672 (1998).
[16]M. Orihashi, Y. Noda, L. Chen, and T. Hirai, Mater. Trans. JIM **41**, 1282 (2000).
[17]L. Fu, J. Cui, Y. Yu, Y. Huang, Y. Wang, Y. Chen, and J. He, J. Mater. Chem. A **7**, 6304 (2019).
[18]S. Aminorroaya Yamini, H. Wang, D. Ginting, D. R. G. Mitchell, S. X. Dou, and G. J. Snyder, ACS Appl. Mater. Interfaces **6**, 11476 (2014).
[19]M. Guch, C. R. Sankar, J. R. Salvador, G. P. Meisner, and H. Kleinke, J. Appl. Phys. **111**, 063706 (2012).
[20]J. He, J. R. Sootsman, S. N. Girard, J.-C. Zheng, J. Wen, Y. Zhu, M. G. Kanatzidis, and V. P. Dravid, J. Am. Chem. Soc. **132**, 8669 (2010).
[21]Y. Gelbstein, Z. Dashevsky, and M. P. Dariel, Physica B **363**, 196 (2005).
[22]Y. Pei, Z. M. Gibbs, A. Gloskovskii, B. Balke, W. G. Zeier, and G. J. Snyder, Adv. Energy Mater. **4**, 1400486 (2014).
[23]Y. I. Ravich, B. A. Efimova, and I. A. Smirnov, *Semiconducting Lead Chalcogenides*, Monographs in Semiconductor Physics Vol. 5, edited by L. S. Stil'bans (Springer Science+Business Media, New York, 1970).
[24]X. Tan, H. Shao, T. Hu, G.-Q. Liu, and S.-F. Ren, J. Phys. Condens. Matter **27**, 095501 (2015).
[25]Y. Xiao *et al.*, J. Am. Chem. Soc. **139**, 18732 (2017).
[26]Y. Xiao, D. Wang, B. Qin, J. Wang, G. Wang, and L.-D. Zhao, J. Am. Chem. Soc. **140**, 13097 (2018).